PAPER • OPEN ACCESS

Two-point Stokes vector diagnostic approach for characterization of optically anisotropic biological tissues

View the article online for updates and enhancements.

Two-point Stokes vector diagnostic approach for characterization of optically anisotropic biological tissues

Motahareh Peyvasteh[1] (ID)**, Alexander Dubolazov**[2]**, Alexey Popov**[3] (ID)**, Alexander Ushenko**[2]**, Yuriy Ushenko**[2] **and Igor Meglinski**[1,4,5,6,7] (ID)

[1] Opto-Electronic and Measurement Techniques Research Unit, University of Oulu, P.O. Box 4500, 90014, Oulu, Finland

[2] Optics and Publishing Department, Chernivtsi National University, 2 Kotsiubynskyi Str., 58012, Chernivtsi, Ukraine

[3] VTT Technical Research Centre of Finland, 90590, Oulu, Finland

[4] Aston Institute of Materials Research, School of Engineering and Applied Science, Aston University, B4 7ET, Birmingham, United Kingdom

[5] School of Life and Health Sciences, Aston University, B4 7ET, Birmingham, United Kingdom

[6] Interdisciplinary Laboratory of Biophotonics, National Research Tomsk State University, 634050, Tomsk, Russia

[7] Institute of Engineering Physics for Biomedicine (PhysBio), National Research Nuclear University 'MEPhI', 15409, Moscow, Russia

E-mail: alexey.popov@vtt.fi and i.meglinski@aston.ac.uk

Abstract

The purpose of the study is to demonstrate a new method of Stokes-correlometric evaluation of polarization-inhomogeneous images of optically thin (optical thickness smaller than 0.01) histological sections from optically anisotropic biological tissues of different morphological structure. This method is based on a correlation ('two-point') generalization of traditional optical methods for analyzing 'one-point' distributions of polarization states of microscopic images of biological tissues. Analytical algorithms are obtained for describing the 'two-point' complex parameters of the Stokes vector image of a birefringent biological tissue. An experimental technique has been developed for measuring polarization-correlation maps, i.e. the coordinate distributions of the magnitude and phase of the 'two-point' Stokes vector parameters. Within the framework of the statistical and correlation analysis of the obtained data, new quantitative criteria for the differentiation of the optical properties of biological tissues of various morphological structures are found. A comparative analysis of the distribution of the 'single-point' and 'two-point' parameters of the Stokes vector of polarizationally inhomogeneous images was performed. It revealed a higher sensitivity (2–5 times) of the Stokes-correlometry method to variations in orientation-phase structure of biological tissues compared to the single-point approach.

Some figures may appear in colour only in the online journal

1. Introduction

Polarization methods occupy an important place in the diagnosis and visualization of the optically anisotropic component of biological tissues [1–5]. For the most complete

description of the interaction of polarized light with such complex objects, the Stokes vector-parametric formalism is used [6–11]. Stokes polarimetry is based on the principles of 'single-point' mapping, i.e. obtaining coordinate distributions (maps) of the azimuth and polarization ellipticity at points of microscopic images of histological sections of biological tissues [12–17]. In the framework of statistical, correlation and fractal analysis of polarization maps, objective criteria for differential diagnosis of various stages of pre-cancer and cancer of human tissues were found [4, 6, 7, 12–17]. However, development of practical applications of the methods of 'single-point' Stokes polarimetry limits the azimuthal dependence of the magnitude of the polarization parameters on the rotation of the plane of the sample of biological tissue relative to the incident laser beam. One of the directions in solving this problem may be the use of the azimuthally invariant correlation approach in polarimetric diagnostics. In [18], a new 'two-point' analytic parameter (complex degree of mutual polarization, CDMP) was proposed to describe the degree of matching of polarization states at various points of optical fields.

This polarization-correlation approach was developed and successfully used for a group of differentiating pathological changes in optical anisotropy of representative samples of histological sections of biological tissues [19, 20]. At the same time, the further development and diagnostic application of new 'two-point' methods of polarization correlometry of the biological tissue structure of various morphological structures and physiological conditions requires overcoming a number of unresolved problems:

(a) improvement of 'CDMP theory' using more general 'two-point' formalism of the Stokes vector theoretically introduced in [21, 22];
(b) development of universal methods for measuring coordinate distributions of 'two-point' parameters of the Stokes vector (polarization-correlation maps) of polarization-inhomogeneous object fields of biological tissues;
(c) obtaining and substantiation of new diagnostic relationships between optically anisotropic structures of biological tissues and their polarization-correlation maps ('Stokes-correlometry parameters', SCP). Our work is aimed at theoretical substantiation and experimental testing of the diagnostic capabilities of the 'two-point' method of Stokes correlometry with the aim of differentiating polarization-correlation SCP maps of optically thin (optical thickness smaller than 0.01) histological sections of biological tissues with different spatial-angular structures of the optically anisotropic component.

2. Theoretical background

Let us consider the object field of an optically anisotropic biological layer. The complex amplitudes $E(r)$ of each point r of such a field are described by the Jones vector [4, 12, 13] in the following form:

$$E(r) = \begin{pmatrix} E_x \\ E_y \end{pmatrix}(r) = \begin{pmatrix} |E_x| \\ |E_y| \exp(\delta_y - \delta_x) \end{pmatrix}(r)$$
$$= \begin{pmatrix} 1 \\ tg\rho(\cos\delta + i\sin\delta) \end{pmatrix}(r). \tag{1}$$

Here, ρ is orientation of optical axis; $tg\rho(r) = \frac{|E_y|(r)}{|E_x|(r)}$ and $\delta(r) = (\delta_y - \delta_x)(r)$ are phase shifts between the orthogonal components $(|E_x|(r), |E_y|(r))$ of laser wave amplitude.

To describe the correlation structure of the stationary distributions of the fields of complex amplitudes of laser radiation converted by optically anisotropic layers, a biological matrix of mutual spectral density can be used in the following form [21, 22]:

$$W_{i,j}(r_1, r_2) = E_i^*(r_1) \cdot E_j(r_2), i, j = x, y. \tag{2}$$

Here r_1 and r_2 are coordinates of the neighboring points in the laser radiation field.

Using this matrix operator one can introduce the following relations for the 'two-point' Stokes vector parameters

$$S_1 = W_{xx}(r_1, r_2) + W_{yy}(r_1, r_2); \tag{3}$$

$$S_2 = W_{xx}(r_1, r_2) - W_{yy}(r_1, r_2); \tag{4}$$

$$S_3 = W_{xy}(r_1, r_2) + W_{yx}(r_1, r_2); \tag{5}$$

$$S_4 = i[W_{yx}(r_1, r_2) + W_{xy}(r_1, r_2)]. \tag{6}$$

Here

$$\begin{cases} W_{xx}(r_1, r_2) = E_x^*(r_1)E_x(r_2); \\ W_{yy}(r_1, r_2) = E_y^*(r_1)E_y(r_2); \\ W_{xy}(r_1, r_2) = E_x^*(r_1)E_y(r_2); \\ W_{yx}(r_1, r_2) = E_y^*(r_1)E_x(r_2). \end{cases} \tag{7}$$

It is known that the first Stokes vector parameter characterizes the full intensity at the point r; the second $S_2(r)$ and third $S_3(r)$ ones characterize changes in polarization azimuth and ellipticity, and the fourth $S_4(r)$ one characterize the value of polarization ellipticity. On this basis we will carry out further detailed analytical and experimental analysis of the potentiality of polarimetry of 'two-point' Stokes vector parameters using $S_3(r_1, r_2)$ and $S_4(r_1, r_2)$ as examples.

Further, for simplification (without reducing completeness of the analysis) we will consider relations (1)–(7) in the approximation of a weak phase modulation ($\delta_i \leqslant 0, 12$; $\cos(\delta_1 - \delta_2) \to 1$; $\sin(\delta_1 - \delta_2) \to \delta_1 - \delta_2$). Please note that this assumption is not artificial for optically thin histological sections of biological tissues. It can be shown that for laser radiation with the wavelength of $\lambda = 0.63\,\mu m$ within

geometrical thickness $l = 30\,\mu m$ of completely optically-anisotropic birefringent layer of biological tissue (value of birefringence $\Delta n \approx 10^{-4} \div 1.5 \times 10^{-3}$ [4, 15, 17]) the maximal phase shift ($\delta_{12} \equiv \delta = \frac{2\pi}{\lambda}\Delta n l$, l—geometrical thickness) is $0.03 \leqslant \delta \leqslant 0.45$. Moreover, among birefringent networks or 'islets' (clusters of spatially non-oriented protein fibers and bundles) there are variations of transverse dimensions of birefringent ($2\,\mu m \leqslant \Delta l \leqslant 20\,\mu m$) structures, which cause weak phase modulation ($2\,\mu m \leqslant \Delta\delta \leqslant 20\,\mu m$) in the plane of a polarizationally inhomogeneous image.

Under these conditions dependences (5) and (6) are reduced to:

$$\begin{cases} |S_3| = 1 - ctg\rho_2\,tg\rho_1; \\ |S_4| = 1 + ctg\rho_2\,tg\rho_1; \end{cases} \tag{8}$$

$$\begin{cases} ArgS_3 = arctg\left(\dfrac{\delta_2 - \delta_1\,ctg\rho_2\,tg\rho_1}{1 + ctg\rho_2\,tg\rho_1}\right); \\ ArgS_4 = arctg\left(\dfrac{1 + ctg\rho_2\,tg\rho_1}{\delta_1 + \delta_2\,ctg\rho_2\,tg\rho_1}\right). \end{cases} \tag{9}$$

Here $|S_{i=3;4}|$ is SCP modulus, $ArgS_{i=13;4}$ is SCP phase.

It follows from the analysis of the obtained formulas (8) and (9) that the SCP absolute value $|S_{i=3;4}(\Delta x, \Delta y)|$ коорАиНаТНои (x,y) orientation structure $\rho(x,y)$ of polycrystalline networks and structures. The SCP phase $Arg\left(S_{i=3;4}(\Delta x, \Delta y)\right)$ carries information about their birefringence ($\delta(x,y)$). Here $\Delta x, \Delta y$ are the 'steps' of scanning in mutually perpendicular directions (x,y).

In the future, algorithms (8) and (9) will be used in the analysis and forecast of changes in the orientation-phase structure of experimental polarization-correlation SCP maps of the optically anisotropic component of biological tissue samples of different morphological structures.

3. Materials and methods

3.1. Setup

Measurement of the coordinate distribution values is carried using a Stokes-polarimeter, which optical scheme is shown in figure 1 [4].

A low-intensity (W = 5.0 mW) He-Ne laser 1 radiation with a wavelength of 633 nm (Lasos HeNe Laser, Edmund Optics, USA) is used as an optical probe. The collimator 2 consists of two micro lenses, the foci of which coincide. As a result, a parallel illuminating beam is formed—a probe with a diameter of 2 mm. To realize the conditions of azimuthally invariant SCP mapping, a circular polarization of the laser beam is formed.

To this end, we use a multifunctional polarizing filter, which consists of sequentially placed quarter-wave plates 3; 5 (Achromatic True Zero-Order Waveplate (APAW 15 mm, Astropribor, Ukraine) and polarizer 4 (B + W XS-Pro Polarizer MRC Nano, Kaesemann, Germany). Histological section 6 converts the circular polarization of the optical probe according to the topographic structure of the optical anisotropic components of biological tissue.

As a result, a polarization-inhomogeneous image of the biological sample under study is formed. A polarizing micro-objective 7 (CFI Achromat P, focal length: 30 mm, numerical aperture: 0.1, magnification: 4x, Nikon, Japan) projects an image of a histological section of biological tissue 6 into matrix plane ($m \times n = 1280 \times 960$ pixels) of the photosensitive area of the digital CCD-camera 10 (CFI Achromat P, focal length: 30 mm, numerical aperture: 0.1, magnification: 4x, Nikon, Japan).

Achromatic True Zero-Order Waveplate (APAW 15 mm, Astropribor, Ukraine) and a polarizer 9 (B + W XS-Pro Polarizer MRC Nano, Kaesemann, Germany) are placed in front of the pixel matrix. The polarization filter passes various linear and circular polarization states of the image of the biological tissue sample 6. As a result, a set of digital (discretized by total number of pixels) polarization-filtered images of the histological section 6 is formed. Then, using the computer 11, algorithmic calculation of the coordinate distributions of the SCP value is performed.

The method of measuring the absolute value $|(S_{i=3;4}(\Delta x, \Delta y))|$ and the phase $Arg\left(S_{i=3;4}(\Delta x, \Delta y)\right)$ of the SCP consists of the following sequence of steps:

(a) Sample 6 is illuminated by the circularly polarized laser beam 1, which provides a filter consisting of quarter-wave plates 3, 5 and polarizer 4 (figure 1);

(b) The axis of a polarizer-analyzer 9 (in the absence of the quarter wavelength plate 8) is rotated by the angles $\Theta = 0^0, \Theta = 90^0, \Theta = 45^0, \Theta = 135^0$, and the intensities of the transmitted radiation $I_0^\otimes; I_{90}^\otimes; I_{45}^\otimes; I_{135}^\otimes$ are measured;

(c) The values of the 'one-point' first, second and third Stokes vector parameters $S_1^\otimes = I_0^\otimes + I_{90}^\otimes;\ S_2^\otimes = I_0^\otimes - I_{90}^\otimes;\ S_3^\otimes = I_{45}^\otimes - I_{135}^\otimes$ are calculated within each pixel of CCD camera 11.

(d) Quarter-wave plate 8 was placed in front of polarizer-analyzer 9, with its axis of the greatest speed being oriented at the angles of $+45^0$ and -45^0 relative to the transmission plane of the polarizer; intensities $I_\otimes^\otimes; I_\oplus^\otimes$ of the transmitted radiation were measured.

(e) The two-dimensional array of values of the fourth Stokes parameter $S_4^\otimes = I_\otimes^\otimes - I_\oplus^\otimes$ was calculated.

(f) $|S_{i=3}(\Delta x; \Delta y)|; Arg\left(S_{i=3}(\Delta x; \Delta y)\right)$ and $|S_{i=4}(\Delta x; \Delta y)|;$ $Arg\left(S_{i=4}(\Delta x; \Delta y)\right)$ were calculated by the following ratios:

$$\begin{cases} |S_3| = \sqrt{\left[\sqrt{I_0(r_1)I_{90}(r_2)}\cos\delta_2 + \sqrt{I_0(r_2)I_{90}(r_1)}\cos\delta_1\right]^2 + } \\ \qquad \overline{+\left[\sqrt{I_0(r_1)I_{90}(r_2)}\sin\delta_2 - \sqrt{I_0(r_2)I_{90}(r_1)}\sin\delta_1\right]^2}; \\ ArgS_3 = arctg\left(\dfrac{\left[\sqrt{I_0(r_1)I_{90}(r_2)}\sin\delta_2 - \sqrt{I_0(r_2)I_{90}(r_1)}\sin\delta_1\right]}{\left[\sqrt{I_0(r_1)I_{90}(r_2)}\cos\delta_2 + \sqrt{I_0(r_2)I_{90}(r_1)}\cos\delta_1\right]}\right). \end{cases} \tag{10}$$
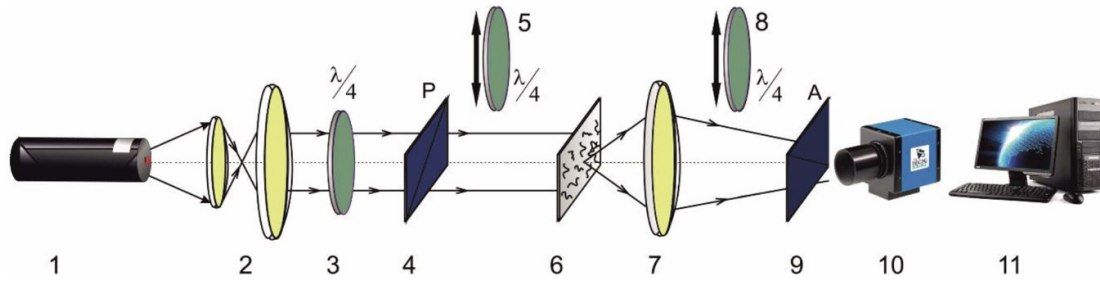
Figure 1. Optical scheme of the polarimeter. 1—He-Ne laser; 2—collimator; 3—stationary quarter-wave plate; 5, 8—mechanically movable quarter-wave plates; 4, 9—polarizer and analyzer; 6—biological sample (layer); 7—polarization micro-objective; 10—CCD camera; 11—computer.

$$\begin{cases} |S_4| = \sqrt{\left[\sqrt{I_0(r_2)I_{90}(r_1)}\sin\delta_1 + \sqrt{I_0(r_1)I_{90}(r_2)}\sin\delta_2\right]^2 +} \\ \quad + \left[\sqrt{I_0(r_2)I_{90}(r_1)}\cos\delta_2 + \sqrt{I_0(r_1)I_{90}(r_2)}\cos\delta_1\right]^2 ; \\ ArgS_4 = arctg\left(\frac{\left[\sqrt{I_0(r_2)I_{90}(r_1)}\cos\delta_2 + \sqrt{I_0(r_1)I_{90}(r_2)}\cos\delta_1\right]}{\left[\sqrt{I_0(r_2)I_{90}(r_1)}\sin\delta_1 + \sqrt{I_0(r_1)I_{90}(r_2)}\sin\delta_2\right]}\right) . \end{cases} \tag{11}$$

$$\delta(r) = arctg\left[\left(\frac{S_4(r)S_2(r)}{S_3(r)}\right)\left(\frac{1 + \frac{I_{90}(r)}{I_0(r)}}{1 - \frac{I_{90}(r)}{I_0(r)}}\right)\right] . \tag{12}$$

Here I_0 and vI_{90} are the intensities at the orientation of transmission plane of polarizer 0^0 and 90^0; δ_i are phase shifts between the orthogonal components of the amplitude of the laser radiation in the points with coordinates r_1 and r_2 [4].

3.2. Biological samples

In the region of 'single-point' polarimetry, relationships were found between the maps of the polarization parameters and the optical anisotropy of the fibrillary and parenchymal structures of biological tissues [1–4, 6, 11, 23]. The information obtained was effectively used in oncology for the differential diagnosis of various stages of cancer [8, 12–17, 24]. Therefore, in our work, we tested the technique of 'two-point' polarization-correlation mapping specifically for these types of biological tissues. This approach makes it possible to conduct a comparative analysis of the sensitivity of various polarimetric techniques and determine the diagnostic potential of Stokes correlometry of pathological changes in the orientation-phase structure of biological tissues.

Histological sections of biological tissues were obtained by a microtome from frozen samples.

The following optically thin (attenuation coefficient $\tau \prec 0.01$) samples of histological sections (geometric thickness $l = 25 \div 30\,\mu m\, 0.0089 \leqslant \tau \leqslant 0.0097$) were studied:

- biological tissues with 'ordered' birefringent fibrillary networks (atrium myocardium—figure 2, fragments (1), (4));
- biological tissues with a 'disordered' birefringent fibrillary networks (ventricle myocardium—figure 2, fragments (2), (5));

- biological tissues—with 'islet' structure (clusters of spatially non-oriented protein fibers) of optically anisotropic formations in the optically isotropic matrix (rectal wall—figure 2, fragments (3), (6)).

The selected samples are ultimate (extreme) types of morphological structure of most human biological tissues, both in orientation and of amorphous-anisotropic structure. This selection of samples will provide comparative information about the patterns and scenarios of changes in the polarization-correlation structure of microscopic images of such objects. This will provide an information basis in the search for relationships between changes in the orientation-phase anisotropy of biological tissue and their polarization-correlation manifestations. The retrieved information can be used for development of new, more sensitive objective criteria for the Stokes-correlometric diagnosis of oncological changes in human organs (formation of spatially oriented fibrillary networks and the growth of birefringence [4, 7, 10, 12, 17, 20]), necrotic changes in the myocardium (degradation fibrillary networks and a decrease in birefringence [12, 13]), inflammatory septic processes (degradation of parenchymal organs—lungs, liver, spleen, kidneys, etc [1, 14, 16, 19]).

Comparative analysis of these microscopic images (figure 2) revealed their individual polarizationally inhomogeneous topographical structure—the coordinate distributions of different polarization states visualized as spots of varying intensity—fragments (4)–(6). Correlation treatment of such polarizationally inhomogeneous images is the basis for a 'two-point' Stokes-polarimetry technique. The aim of such studies is to identify objective statistical, correlation, and fractal criteria that characterize the correlation coherence of optical anisotropy parameters and can be the basis for the differential diagnosis of biological tissues birefringence changes.

3.3. Analysis of experimental data

3.3.1. Statistical analyses. To assess distributions of random values of the module and phase of the 'two-point' parameters of the Stokes vector of polarization-inhomogeneous microscopic images of histological sections of biological tissues a set of central statistical moments of the first and fourth orders (mean Z_1, variance Z_2, skewness Z_3 and kurtosis Z_4) is calculated according to the traditional method presented in [4].
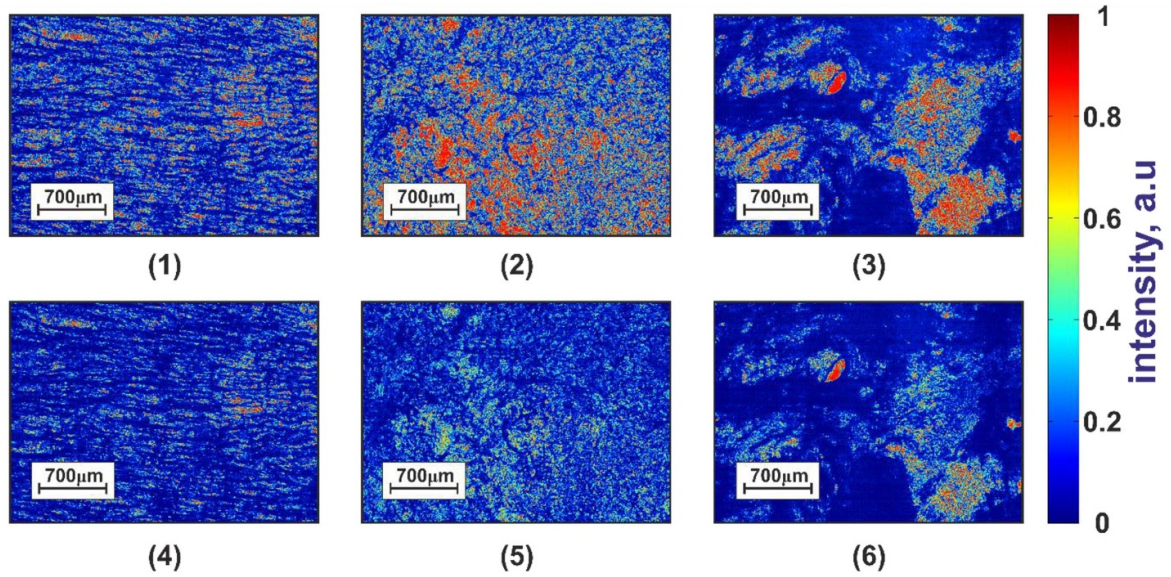
Figure 2. Polarization-inhomogeneous microscopic images of histological sections of biological tissues of different morphological structure: Upper row (coaxial polarizer 4 and analyzer 9 position): spatially ordered fibrillary (1), disordered (2) myosin myocardial networks and islet parenchymal structures of the colon wall (3). Bottom row (crossed polarizer 4 and analyzer 9 position): optically anisotropic structures of myosin myocardial networks ((4), (5)) and colon wall parenchyma (6).

3.3.2. Correlation analysis. The correlation approach in the analysis of polarization-correlation SCP maps of microscopic images of histological sections of biological tissues is based on:

• calculation of the set of autocorrelation functions of SCP-parameters by means of line scanning with a scanning step $\Delta x = 1 pix$ of according to the algorithm given in [12];

• calculation of the resulting autocorrelation function of the coordinate distribution of SCP-parameters by averaging the partial correlation dependencies over all (n) lines $(1, \ldots, m)$ of photosensitive matrix of the CCD camera 10 (figure 1).

3.3.3. Fractal analysis. Fractal analysis of coordinate distributions of SCP-parameters of microscopic images of histological sections of biological tissues is based on:

• row-by-row calculation of the set of partial logarithmic dependences $(\log J(SCP)_{i=m} - \log(\phi))$ of power spectra of random SCP values, where $\phi = d^{-1}$ is spatial frequency defined by the physical sizes (d) of structural elements of SCP-maps;

• averaging over all (n) lines $(1, \ldots, m)$ of photosensitive matrix of the CCD camera 10 (figure 1) partial logarithmic dependences of power spectra of random SCP values;

• determination by the least squares method [15] of an approximating curve $F(\gamma)$ to the resulting logarithmic dependences $(\log J(SCP)_{i=m} - \log(\phi))$;

• fractal (the constant value of slope angle $\gamma = const$ for 2–3 decades of size d changes), multifractal (several constant slope angles) and statistical (absence of several constant slope angles) dependencies $F(\gamma)$ [8, 9, 12];

• calculation of the variance that characterizes the distribution of the resulting logarithmic dependences $(\log J(SCP)_{i=m} - \log(\phi))$.

4. Results and discussion

4.1. Tissue with ordered (rectilinear) birefringent fibrillar networks—myocardium atrium

Figure 3 present 2D distributions of values $|S_{i=3;4}(\Delta x; \Delta y)|$ (figure 3(a)) and $Arg(S_{i=3;4}(\Delta x, \Delta y))$ (figure 3(b)) (fragments (1), (5)), histograms N (fragments (2), (6)), autocorrelation functions $\bar{K}(\Delta x)$ (fragments (3), (7)) and logarithmic $\log J(|S_{i=3;4}(\Delta x; \Delta y)|) - \log(d^{-1})$, $\log J(Arg(S_{i=3;4}(\Delta x; \Delta y))) - \log(d^{-1})$ dependences (fragments (4), (8)) of SCP modulus and phase distributions, calculated for polarizationally inhomogeneous microscopic image of histological section of myocardium atrium.

Analysis of the obtained polarization-correlation maps of the SCP module (figure 3(a)) revealed the following:

• coordinate heterogeneity of the distributions of the magnitude of the third and fourth 'two-point' parameters $|S_{i=3;4}(\Delta x, \Delta y)|$ of the Stokes vector of the microscopic image of a spatially ordered network of myosin fibrils atrium myocardium (figure 3(a), fragments (1), (5));

• histograms of distributions of random variables $|S_{i=3;4}(\Delta x, \Delta y)|$ are individual for the third and fourth 'two-point' parameters (figure 3(a), fragments (2), (6));

• probabilistic distributions N are characterized by the presence of major extrema localized in the vicinity $|S_{i=3;4}(\Delta x, \Delta y)| = 0$, as well as a significant scatter in SCP, asymmetry and peak acuity (figure 3(a), fragments (2), (6));
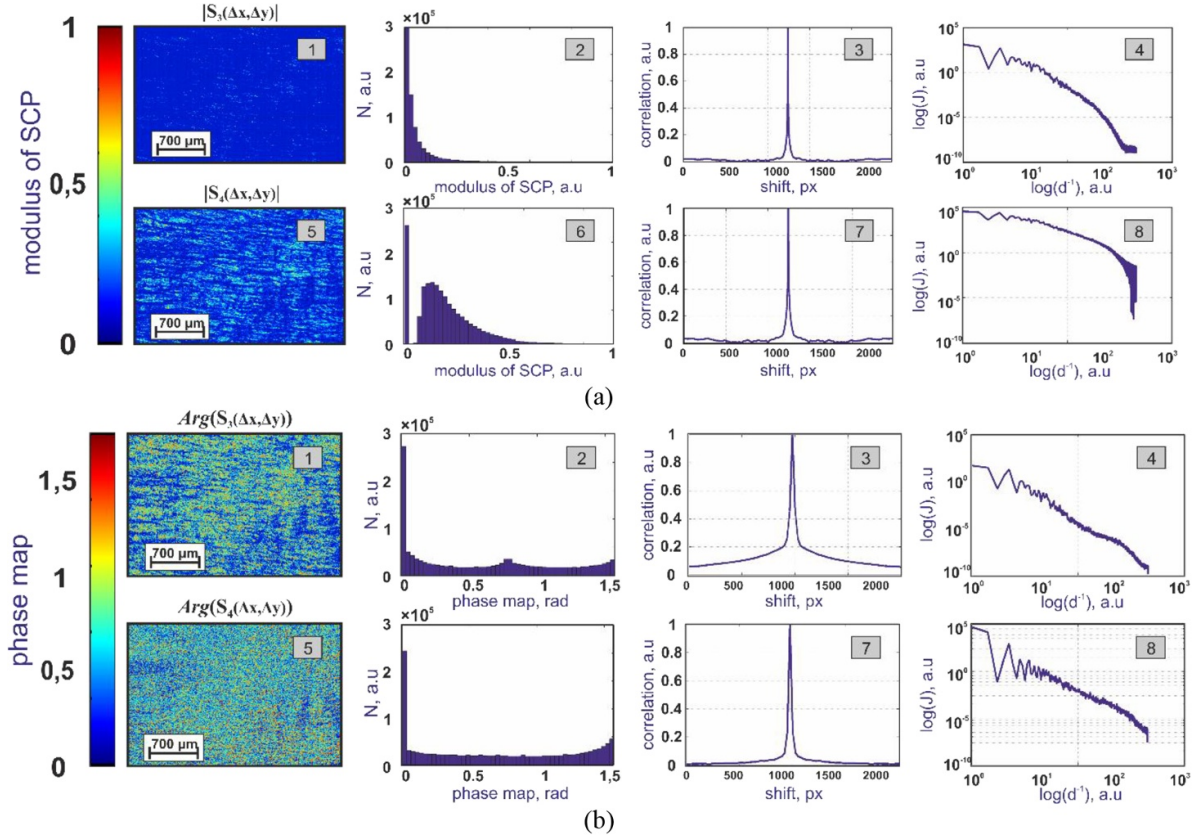
Figure 3. Stokes correlometry of spatially ordered birefringent fibrillary networks. Topographic (fragments (1), (5)), statistical (fragments (2), (6)), correlation (fragments (3), (7)) and fractal (fragments (4), (8)) SCP maps structure of modulus (a) and phase (b) of polarizationally inhomogeneous image of myocardium atrium.

For polarization-correlation maps of the SCP phase of the third and fourth 'two-point' parameters of the Stokes vector (figure 3(b)) the following is found:

● individual and coordinate-inhomogeneous topographic structure of the distribution of quantities $Arg\left(S_{i=3;4}\left(\Delta x, \Delta y\right)\right)$ (figure 3(b), fragments (1), (5));

● high sharpness of the peak, asymmetry, and the range of variation in the phase magnitude of the third and fourth 'two-point' $Arg\left(S_{i=3;4}\left(\Delta x, \Delta y\right)\right)$ parameters relative to the main extrema (figure 3(b), fragments (2), (6)).

From the physical point of view, the results of the experimental structure of the polarization-correlation maps of the module $\left|S_{i=3;4}\left(\Delta x, \Delta y\right)\right|$ can be explained as follows.

In the 'one-point' approximation, the third parameter of the Stokes vector characterizes the magnitude of the polarization azimuth [4, 6]. The magnitude of the polarization azimuth is proportional to the direction of the optical axis ρ (relation (1)) of the biological crystal, which is determined by the spatial orientation of the birefringent fibrils [13, 15, 17]. Therefore, the degree of correlation 'point-to-point' matching ($\left|S_{i=3}\left(\Delta x, \Delta y\right)\right|$) of polarization azimuths at the points of the microscopic image of spatially ordered atrium myocardium myosin fibrils practically does not change.

As a result, the polarization-correlation map of this SCS parameter is quite homogeneous (figure 3(a), fragment (1)),

and the distribution histogram is characterized by a pronounced extremum (figure 3(a), fragment (2)).

The fourth 'one-point' parameter of the Stokes vector characterizes the magnitude of the ellipticity of polarization [4, 11, 12]. This parameter is more pronounced in comparison with the azimuth associated with the direction of the optical axis ρ of the birefringent fibrils (relation (1)). Therefore, the degree of correlation 'point-to-point' matching ($\left|S_{i=4}\left(\Delta x, \Delta y\right)\right|$) of the ellipticity of polarization at the points of the microscopic image of myosin fibrils of myocardium atrium is more sensitive to variations ρ.

As a result, the degree of correlation matching of the ellipticity of polarization at different points decreases. As a result, the coordinate heterogeneity of the polarization-correlation maps of this SCP parameter (figure 3(a), fragment (5)) increases, and additional 'decorrelation' extremes (figure 3(a), fragment (6)) are formed in the distribution histogram.

The topographic and statistical structure of the polarization-correlation maps of the phase of the 'two-point' parameters $Arg\left(S_{3;4}\left(\Delta x, \Delta y\right)\right)$ of the Stokes vector are similar (figure 3(b), fragments (1), (2), (5), (6)).

The experimentally obtained structure of polarization-correlation maps of the modulus $\left|S_{i=3;4}\left(\Delta x, \Delta y\right)\right|$ and phase $Arg\left(S_{i=3;4}\left(\Delta x, \Delta y\right)\right)$ is in good agreement with the developed model representations of the processes of formation of the magnitude of the third and fourth 'two-point' parameters of

the Stokes vector of the microscopic image of a birefringent spatially ordered network of atrium myocardium myosin fibrils.

The results can be associated with the following physical considerations. The values of SCP modulus $|S_{i=3;4}(\Delta x, \Delta y)|$ (figure 3(a), fragments (1), (5)) are primarily defined by the directions of the optical axes ρ in the neighboring points r_1 and r_2 of the plane of the histological sections (equations (8) and (9)). For biological tissue with rectilinear packaging of myosin fibrils, in the extreme case the differences between $\rho(r_1)$ and $\rho(r_2)$ are minor $(\rho(r_1) - \rho(r_2) \to 0)$. So, most likely the following values of the modulus $|S_{i=3}(\Delta x, \Delta y)| \to 0$ and $|S_{i=4}(\Delta x, \Delta y)| \to 1$ (equations (8) and (9)), which form the core extremes of histograms $N(|S_{i=3;4}(\Delta x, \Delta y)|)$ (figure 3(a), fragments (2), (6)) are probable. However, for real myocardial tissue of this type there is always a certain number of curved fibrils, packed differently. For such birefringent networks there is a certain condition $\rho(r_1) - \rho(r_2) \neq 0$. Thus a set of other SCP modulus values is formed. Quantitatively, this scenario appears in the redistribution of the entire range $0 \leqslant |S_{i=3;4}(\Delta x, \Delta y)| \leqslant 1$ of values $|S_{i=3;4}(\Delta x, \Delta y)|$ (figure 3(a), fragment (2)). Furthermore, an additional extreme of the histogram $N(|S_{i=4}(\Delta x, \Delta y)|)$ is formed (figure 3(a), fragment (6)).

The SCP phase value $Arg(S_{3;4}(\Delta x, \Delta y))$ (figure 3(b), fragments (1), (5)) is determined by the degree of coordinate coherence of both the directions of the geometry axes $\rho(r)$ of myocardium myosin fibrils and the value of the phase shift between the orthogonal components of the amplitude of laser radiation (equations (8), (9)). It comes from the analysis of the above relations that the extreme values $Arg(S_3(\Delta x, \Delta y)) \to 0$ and $Arg(S_4(\Delta x, \Delta y)) \to 0.5\pi$ are determined by these orientation-phase conditions $\begin{pmatrix} \rho(r_1) \approx \rho(r_2); \\ \delta(r_1) \approx \delta(r_2) \end{pmatrix}$ fulfilment. Such conditions are most probable particularly for the ensemble of myosin fibrils of the ordered birefringent network. Quantitatively, this is confirmed by the formation of major extremes of histograms $N(Arg(S_3(\Delta x, \Delta y)) = 0)$ and $N(Arg(S_4(\Delta x, \Delta y)) = 0.5\pi)$ (figure 3(b), fragments (2), (6)). However, this mechanism is not the only one. The value of the phase shift is also changing due to the difference in the size of birefringent fibrils and their curvature. As a result of these two factors a wide range of values $(0 \leqslant Arg(S_{i=3;4}(\Delta x, \Delta y)) \leqslant 0.5\pi)$ change of SCP phase is formed in polarizationally inhomogeneous image of *myocardium atrium* histological sections (figure 3(b), fragments (2), (6)).

4.2. Tissue with disordered birefringent fibrillar networks—myocardium ventricle

In the series of dependencies in figure 4 the statistical, correlation and fractal characteristics of values $|S_{i=3;4}(\Delta x; \Delta y)|$ distributions (figures 4(a) and $Arg(S_{i=3;4}(\Delta x; \Delta y))$ (b), calculated for histological sections of myocardium ventricle with the network of myosin fibers disordered by the packaging directions are presented.

A physical analysis of the data of polarization-correlation mapping (figure 4(a)) of the coordinate distributions of the magnitude of the 3rd and 4th 'two-point' parameters of the Stokes vector of a microscopic image of a histological section of myocardium ventricle revealed:

● an increase in the coordinate heterogeneity of the distributions of the quantity $|S_{i=3;4}(\Delta x; \Delta y)|$ (figure 4(a), fragments (1), (5)) in comparison with the Stokes correlometry data of the microscopic image of the histological section of myocardium atrium (figure 3(a), fragments (1), (5));

● a decrease in the magnitude of the main extrema that characterize the histograms of the distribution of parameters $|S_{i=3;4}(\Delta x; \Delta y)|$ and the formation of additional local extrema (figure 4(a), fragments (2), (6));

Topographic (fragments (1), (5)), statistical (fragments (2), (6)), correlation (fragments (3), (7)) and fractal (fragments (4), (8)) SCP maps structure of modulus (a) and phase (b) of polarizationally inhomogeneous image of myocardium ventricle.

The revealed scenario of transformation of the topographic and statistical structure of the distributions of the magnitude of the 3rd and 4th 'two-point' parameters of the Stokes vector of the microscopic image of the histological section of myocardium ventricle can be associated with a wider range of spatial orientations of the optical axes of myosin fibrils. As a result, at the points of a polarization-inhomogeneous image of a myocardial sample of this type, the degree of correlation between the azimuth and ellipticity of polarization decreases.

For polarization-correlation maps of the SCP phase of parameters (figure 4(b)), similar processes of transformation of coordinate (figure 4(b), fragments (1), (5)) and probability (figure 4(b), fragments (2), (6)) distributions of the value $Arg(S_{i=3;4}(\Delta x; \Delta y))$ are revealed. This scenario is caused by an increase in the dispersion of orientations ρ of the optical axes and phase shifts δ introduced by birefringent myosin fibrils of various geometric thicknesses (relation (1)).

As a result of the analysis (figures 4(a), and (b) of the obtained data concerning the SCP-maps structure (fragments (1), (5)) the increase of decorrelation degree between the values of Stokes vector parameters at the points of the polarizationally inhomogeneous image of myocardium ventricle are detected. Quantitatively, it is manifested in the reduction of peak sharpness of histograms $N(|S_{i=3}(\Delta x; \Delta y) = 0|)$ and $N(|S_{i=4}(\Delta x; \Delta y) = 1|)$, and in the increase of the value of the additional extremum $(|S_{i=4}(\Delta x; \Delta y)| \neq 0)$ of distributions $N(|S_{i=4}(\Delta x; \Delta y)|)$ (figure 4(a), fragments (2), (6)). In addition, the major extremes of histograms $N(Arg(S_{i=3}(\Delta x; \Delta y) = 0))$ and $N(Arg(S_{i=4}(\Delta x; \Delta y) = 0.5\pi))$ are reduced, and the probability of SCP phase values $Arg(S_{i=3;4}(\Delta x; \Delta y))$ different from the boundary ones $(0; 0.5\pi)$ increases (figure 4(b), fragments (2), (6)).

Physically detected features can be related to the influence of two factors. The first factor is the increase in the range of optical axes ρ orientations, determined by the packaging directions of birefringent myosin fibrils. As a result of the increase in differences between $\rho(r_1)$ and $\rho(r_2)$ the following tendency of the values of $|S_{i=3}(\Delta x; \Delta y)| \uparrow$ and
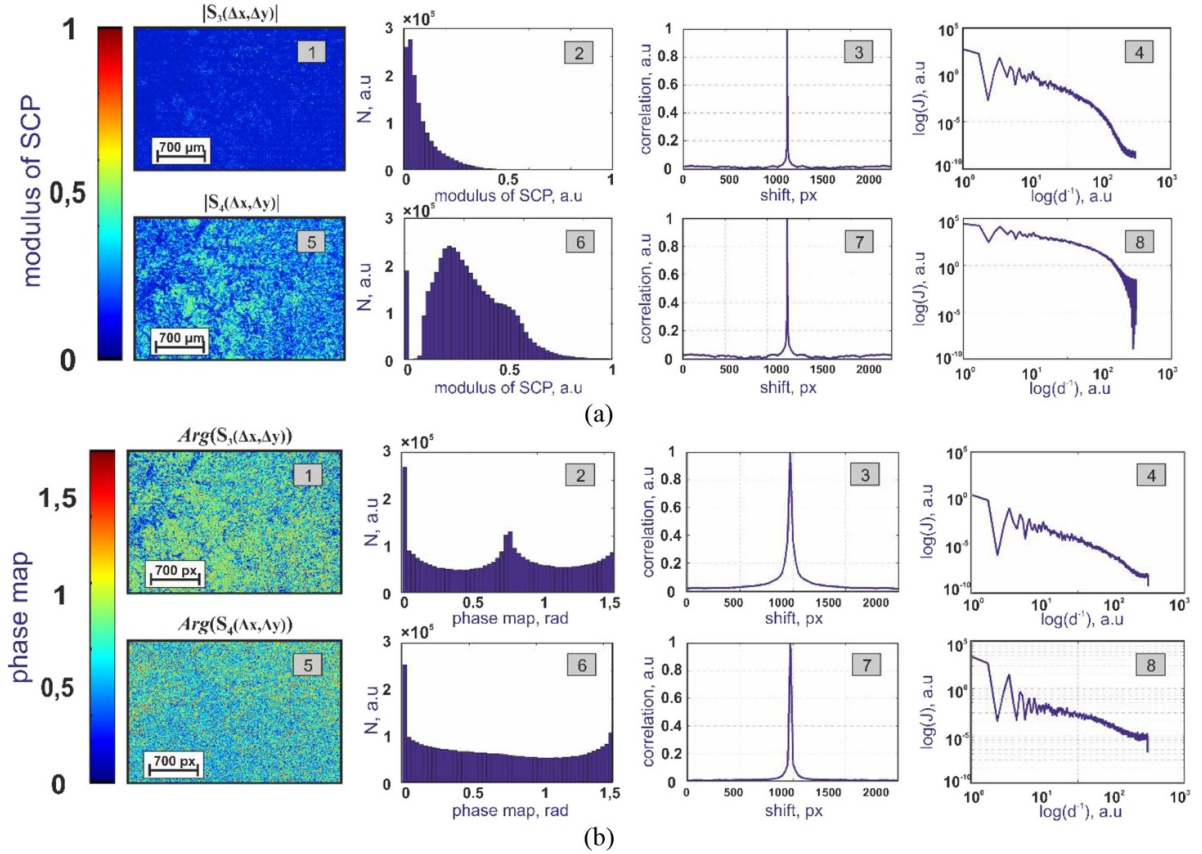
Figure 4. Stokes-correlometry of spatially disordered birefringent fibrillary networks.

$|S_{i=4}(\Delta x; \Delta y)| \downarrow$ increase is observed (equations (8), (9)). The second factor is the increase of spatial frequency of phase modulation $\delta(\Delta x, \Delta y)$ due to the geometry of disordered fibrillary network of this type of tissue—$Arg(S_{i=3}(\Delta x; \Delta y)) \uparrow$ and $Arg(S_{i=4}(\Delta x; \Delta y)) \downarrow$ (equation (9)).

4.3. Tissue with 'islet' structure of optically anisotropic formations—the rectum wall

Figure 5 show the maps $|S_{i=3;4}(\Delta x; \Delta y)|$ (figure 5(a), fragment (1)) and (figure 5(b), fragment (1)), the distribution histograms $N(|S_{i=3;4}(\Delta x; \Delta y)|), N(Arg(S_{i=3;4}(\Delta x; \Delta y)))$ (fragments (2) (6)), autocorrelation $\bar{K}(|S_{i=3;4}(\Delta x; \Delta y)|), \bar{K}(Arg(S_{i=3;4}(\Delta x; \Delta y)))$ (fragments (3) (7)) and logarithmic $\log J(|S_{i=3;4}(\Delta x; \Delta y)|) - \log(d^{-1}), \log J(Arg(S_{i=3;4}(\Delta x; \Delta y))) \log(d^{-1})$ dependences (fragments (4), (8)) calculated for the histological sections of rectal wall.

As it is seen from the analysis of the SCP maps (figures 5(a) and (b), fragments (1), (5)) the polarizationally inhomogeneous image of parenchymal tissue shows a significant increase in the level of correlation between the values of the Stokes vector parameters. Quantitatively, it illustrates the growth of the peaks sharpness in histograms $N(|S_{i=3}(\Delta x; \Delta y)| = 0)$ and $N(|S_{i=4}(\Delta x; \Delta y)| = 1)$ (figure 5(a), fragments (2), (6)) as well as $N(Arg(S_{i=3}(\Delta x; \Delta y)) = 0)$ and $N(Arg(S_{i=4}(\Delta x; \Delta y)) = 0.5\pi)$ (figure 5(b), fragments (2), (6)) and reduction of the additional extremum

$(|S_{i=4}(\Delta x; \Delta y)| \neq 0)$ of distribution $N(|S_{i=4}(\Delta x; \Delta y)|)$ (figure 5(a), fragment (6)).

From the physical point of view the determined features of the statistical structure of SCP-maps can be associated with having a significant impact of optically isotropic component in the substance of histological sections of rectal wall (figure 5(a), fragments (2), (6)). Within these areas the field in the plane of the microscopic image is polarizationally homogeneous. Thus the consistency of the Stokes vector parameters is maximal: $\begin{pmatrix} \rho(r_1) = \rho(r_2) = 0; \\ \delta(r_1) = \delta(r_2) = 0 \end{pmatrix}$. Due to this the probability of extreme values of $|S_{i=3}(\Delta x; \Delta y)| = 0; |S_{i=4}(\Delta x; \Delta y)| = 1$ and $Arg(S_{i=3}(\Delta x; \Delta y)) = 0; Arg(S_{i=4}(\Delta x; \Delta y)) = 0.5\pi$ in the total distribution of the SCP modulus and phase value of the corresponding microscopic image of the rectal wall histological sections significantly increases.

4.4. Correlation analysis of SCP-maps

As it was mentioned above, in each point (r) of polarizationally non-uniform microscopic images of histological sections of myocardium and amorphous anisotropic rectum wall, an individual value of Stokes vector parameters $S_i(r)$ is formed. In other words, the SCP-maps $(S_{i=3;4}(\Delta x; \Delta y))$ and $Arg(S_{i=3;4}(\Delta x, \Delta y))$ are also coordinately inhomogeneous. This fact is substantiated by the rapid decrease of autocorrelation functions $\bar{K}((|S_{i=3;4}(\Delta x; \Delta y)|))$
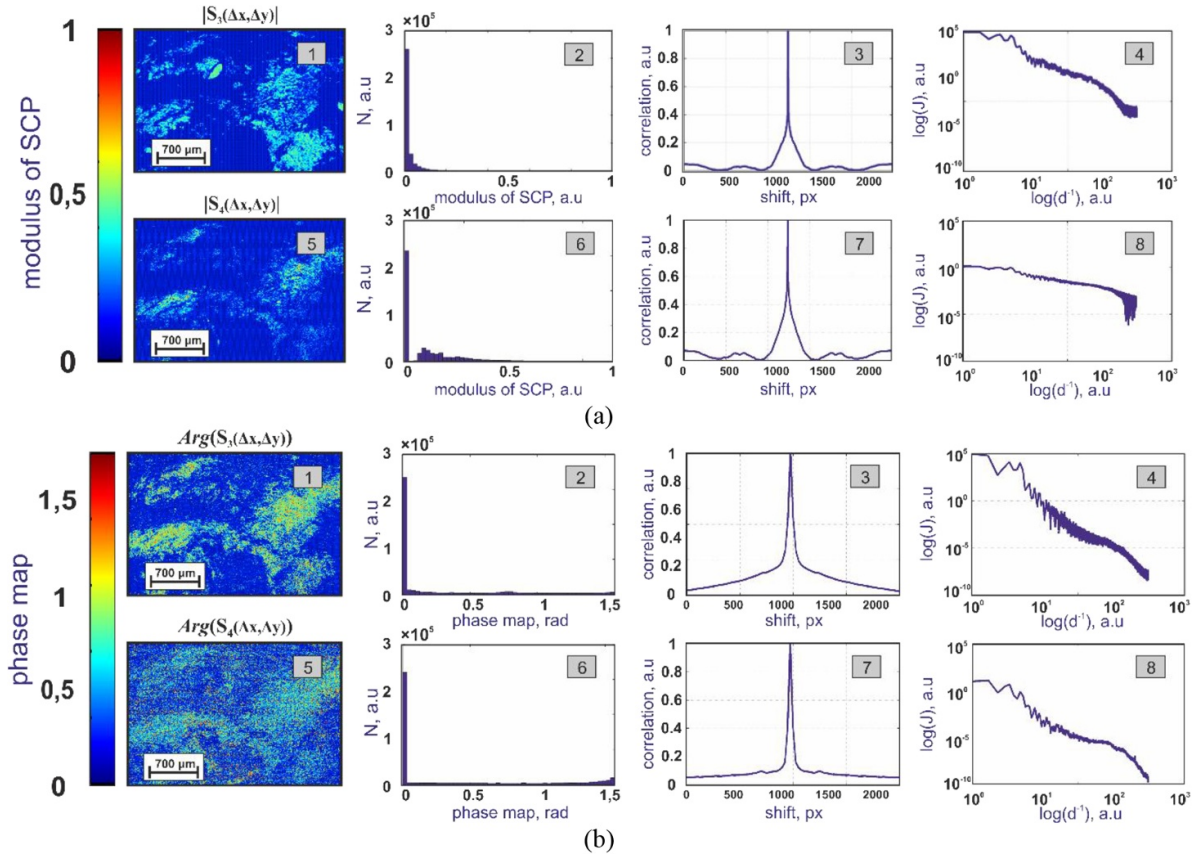
Figure 5. Stokes correlometry of parenchymal optically anisotropic tissues. Topographic (fragments (1), (5)), statistical (fragments (2), (6)), correlation (fragments (3), (7)) and fractal (fragments (4), (8)) SCP maps structure of modulus (a) and phase (b) polarizationally inhomogeneous image of rectum wall.

Table 1. Statistical, correlation and fractal parameters SCP modulus maps.

Parameters, q	Myocardium tissue (ordered) ($n = 39$)		Myocardium tissue (disordered) ($n = 39$)		Rectum wall ($n = 39$)	
$|S_{i=3;4}(\Delta x; \Delta y)|$	S_3	S_4	S_3	S_4	S_3	S_4
Z_1	0.04 ± 0.002	0.81 ± 0.041	0.081 ± 0.038	0.62 ± 0.057	0.019 ± 0.009	0.51 ± 0.032
Z_2	0.006 ± 0.0003	0.01 ± 0.0046	0.004 ± 0.0002	0.009 ± 0.0005	0.002 ± 0.0001	0.0078 ± 0.0003
Z_3	1.16 ± 0.057	1.09 ± 0.049	3.76 ± 0.16	1.49 ± 0.078	5.38 ± 0.29	1.88 ± 0.098
Z_4	4.05 ± 0.23	1.25 ± 0.063	13.88 ± 0.88	2.18 ± 0.12	43.5 ± 2.88	4.76 ± 0.27
Z_2^k	0.11 ± 0.006	0.14 ± 0.008	0.13 ± 0.007	0.15 ± 0.008	0.13 ± 0.005	0.11 ± 0.004
$\pm$	1.14 ± 0.06	1.26 ± 0.07	1.46 ± 0.08	0.98 ± 0.045	1.27 ± 0.06	0.74 ± 0.033
D^f	0.27 ± 0.016	0.25 ± 0.011	0.34 ± 0.016	0.32 ± 0.012	0.21 ± 0.013	0.17 ± 0.008

Table 2. Statistical, correlation and fractal parameters SCP phase maps.

Parameters, q	Myocardium tissue (ordered) ($n = 39$)		Myocardium tissue (disordered) ($n = 39$)		Rectum wall ($n = 39$)	
$Arg(S_{i=3;4}(\Delta x; \Delta y))$	S_3	S_4	S_3	S_4	S_3	S_4
Z_1	0.11 ± 0.006	1.17 ± 0.05	0.21 ± 0.01	0.91 ± 0.053	0.29 ± 0.015	0.74 ± 0.042
Z_2	0.27 ± 0.012	0.3 ± 0.014	0.22 ± 0.011	0.25 ± 0.013	0.21 ± 0.011	0.23 ± 0.012
Z_3	0.34 ± 0.014	0.13 ± 0.007	0.74 ± 0.036	0.37 ± 0.015	1.39 ± 0.037	1.07 ± 0.055
Z_4	1.25 ± 0.037	1.05 ± 0.027	1.85 ± 0.093	1.87 ± 0.098	2.57 ± 0.13	2.63 ± 0.14
Z_2^k	0.11 ± 0.005	0.14 ± 0.006	0.13 ± 0.006	0.15 ± 0.007	0.13 ± 0.006	0.11 ± 0.005
Z_4^k	1.14 ± 0.052	1.26 ± 0.061	1.46 ± 0.071	0.98 ± 0.044	1.27 ± 0.058	0.74 ± 0.034
D^f	0.34 ± 0.014	0.24 ± 0.011	0.34 ± 0.014	0.21 ± 0.01	0.25 ± 0.013	0.17 ± 0.08

Table 3. Statistical, correlation and fractal maps of Stokes vector $S_{i=3;4}$ parameters of polarizationally inhomogeneous images of biological tissues.

Parameters, q $S_{i=3;4}$	Myocardium tissue (ordered) ($n = 39$)		Myocardium tissue (disordered) ($n = 39$)		Rectum wall ($n = 39$)	
	S_3	S_4	S_3	S_4	S_3	S_4
Z_1	0.32 ± 0.012	0.19 ± 0.01	0.26 ± 0.011	0.18 ± 0.051	0.21 ± 0.01	0.16 ± 0.006
Z_2	0.16 ± 0.008	0.09 ± 0.0043	0.13 ± 0.007	0.11 ± 0.005	0.14 ± 0.007	0.086 ± 0.004
Z_3	0.56 ± 0.027	0.69 ± 0.034	0.71 ± 0.033	0.79 ± 0.038	0.98 ± 0.042	1.03 ± 0.058
Z_4	0.65 ± 0.034	0.72 ± 0.043	0.78 ± 0.048	0.98 ± 0.052	1.25 ± 0.068	1.47 ± 0.071
Z_2^k	0.14 ± 0.007	0.16 ± 0.008	0.17 ± 0.008	0.15 ± 0.007	0.18 ± 0.009	0.13 ± 0.004
Z_4^k	0.81 ± 0.056	0.96 ± 0.067	0.94 ± 0.078	1.19 ± 0.065	0.77 ± 0.046	0.65 ± 0.038
D^f	0.23 ± 0.012	0.21 ± 0.011	0.36 ± 0.019	0.29 ± 0.015	0.27 ± 0.013	0.21 ± 0.011

and $\bar{K}\left(Arg\left(S_{i=3;4}\left(\Delta x; \Delta y\right)\right)\right)$ (figures 3(b)–5, fragments (3), (7)). Comparative analysis of such dependencies showed the most rapid 'decrease' for the sample of myocardium with the structure disordered by the directions of birefringent myosin fibrils (figures 4(a) and (b), fragments (3), (7)). The autocorrelation functions of the distributions $\left|S_{i=3;4}\left(\Delta x; \Delta y\right)\right|$ defined for the polarizationally inhomogeneous image of rectal wall (figures 5(a) and (b), fragments (3), (7)) are the slowest in decrease. This may be related to the lowest period of the coordinate modulation of the values of modulus and phase of the SCP image of myocardium ventricle (figure 5(a), fragments (1), (5)) due to the largest variance of birefringence parameters. On the contrary, for amorphous anisotropic tissue of rectum wall (figure 5(b), fragments (3), (7)) fluctuations of such parameters are significantly lower or minimal. Due to this fact, the sharpness of the peak of autocorrelation function $\bar{K}\left(\left|S_{i=3;4}\left(\Delta x; \Delta y\right)\right|\right)$ and $\bar{K}\left(Arg\left(S_{i=3;4}\left(\Delta x; \Delta y\right)\right)\right)$ decreases, while the half-width increases. In other words, the statistical moments of the 2nd and 4th order can be selected as the objective criteria of changes in the topographic structure of distributions $\left|S_{i=3;4}\left(\Delta x; \Delta y\right)\right|$ and $Arg\left(S_{i=3;4}\left(\Delta x, \Delta y\right)\right)$ that will be further referred to as correlation moments Z_2^k and Z_4^k.

4.5. Fractal analysis of SCP-map

It is known that the geometry of fibrillary and polycrystalline structures of most biological tissues is hierarchical or self-similar in scale. In particular, for filamentous protein networks this is implemented in the following hierarchical sequence—'polypeptide chain—microfibril—fibril—fiber—bundle' [4, 12]. On this basis we should expect the formation of fractal or multifractal distributions of values of not only polarization parameters, but also of the polarization-correlation ones of microscopic images of biological layers. Within Stokes-correlometry mapping it was determined that experimentally measured SCP-maps ($\left|S_{i=3;4}\left(\Delta x; \Delta y\right)\right|$ and $Arg\left(S_{i=3;4}\left(\Delta x; \Delta y\right)\right)$) have fractal or multifractal structure. The approximating lines to the logarithmic dependences of power spectra $\log J\left(\left|S_{i=3;4}\left(\Delta x, \Delta y\right)\right|\right) - \log\left(d^{-1}\right)$ and $\log J\left(Arg\left(S_{i=3;4}\left(\Delta x, \Delta y\right)\right)\right) - \log\left(d^{-1}\right)$ are either straight or broken with two inclination angles (figures 3–5, fragments (6), (8)). The comparative analysis of these dependences shows that the distribution of their values are characterized by the individual value of dispersion D^f. The largest

variation is observed for coordinate distributions of SCP-maps of microscopic images of histological sections of myocardium with disordered birefringent fibrillary network (figures 4(a) and (b), fragments (6), (8)). The smallest variation is observed for polarizationally inhomogeneous image of rectum wall tissue (figures 5(a) and (b), fragments (6), (8)). From a physical point of view it can be associated with the geometric features dimensions of the SCP-maps structural elements. The largest range of changes due to the specific morphological structure of biological tissue is observed for myocardium ventricle; while the smallest one is observed for the amorphous anisotropic tissue of the rectum wall.

4.6. Intergroup statistical, correlation and fractal analysis of the modulus and phase distributions of SCP-maps

The results of statistical ($Z_{i=1;2;3;4}$), correlation ($Z_{i=2;4}^k$) and fractal (D^f) analysis of coordinate distributions of the values of $\left|S_{i=3;4}\left(\Delta x; \Delta y\right)\right|$ and $Arg\left(S_{i=3;4}\left(\Delta x; \Delta y\right)\right)$ of polarizationally inhomogeneous images of histological sections of all types of biological tissues are presented in tables 1 and 2, respectively. For this purpose, three statistically reliable sample groups of biological tissues—39 samples in each group—were formed. Further, within each group the average values of $\bar{q}$ and average errors $\pm\chi$ were calculated.

Analysis of the data presented in tables 1 and 2 show that:

- individual values of statistical $Z_{i=1;2;3;4}$, correlation $Z_{i=2;4}^k$ and fractal D^f parameters describing the coordinate distributions $\left|S_{i=3;4}\left(\Delta x; \Delta y\right)\right|$ and $Arg\left(S_{i=3;4}\left(\Delta x; \Delta y\right)\right)$ for each type of biological tissue;
- the values of statistical moments of the 3rd ($Z_3\left(\left|S_{i=3;4}\right|; Arg\left(S_{i=3;4}\right)\right)$) (3–5 times) and 4th ($Z_4\left(\left|S_{i=3;4}\right|; Arg\left(S_{i=3;4}\right)\right)$) orders (3–10 times), of correlation moment of the 4th ($Z_4^k\left(\left|S_{i=3;4}\right|; Arg\left(S_{i=3;4}\right)\right)$) order (2.2 times) and of dispersion D^f (up to 2.2 times) of logarithmic dependences of power spectra $\log J\left(\left(\left|S_{i=3;4}\right|; Arg\left(S_{i=3;4}\right)\right)\right) - \log\nu$ are maximally different (highlighted in light-gray) for the distributions of the values of the SCP modulus and phase of polarizationally inhomogeneous images of polycrystalline networks of optically thin biological layers of different types.

The obtained results of the Stokes-correlometry mapping were compared with the similar results of the technique of the

Stokes-polarimetry mapping of microscopic images of histological sections of three types for biological tissues samples (table 3).

The Stokes-polarimetry mapping showed that the most sensitive (highlighted in light-gray) to the peculiarities of orientation-phase structure of the studied 'extreme' types of biological tissues were:

- values of statistical moments of the 1st $Z_1(S_{i=3;4})$ (about 1.5–2 times), 3rd $Z_3(S_{i=3;4})$ (about 1.95 times) and 4th $Z_4(S_{i=3;4})$ orders (about 2.5 times);
- values of the correlation moment of the 4th ($Z^k_4(S_{i=3;4})$) order (1.9 times);
- values of dispersion (about 1.6 times) of logarithmic dependences of power spectra $\log J(S_{i=3;4}) - \log \nu$.

5. Conclusions

A new method of Stokes-correlometry is suggested and analytically substantiated. It reveals coordinate distributions of modulus and phase of 'two-point' Stokes vector parameters of polarizationally inhomogeneous images for optically thin (optical thickness smaller than 0.01) histological sections of biological tissues with different morphological structure.

Within statistic, correlation and fractal analysis the objective criteria characterizing the SCP-maps of polarizationally non-uniform microscopic images for three groups of samples (with the ordered, disordered birefringent fibrillary networks and the 'islet' isotropic, anisotropic structure) are revealed.

Comparative analysis of the results based on statistical, correlation and fractal analysis of distributions of 'single-point' and 'two-point' Stokes vector parameters of polarizationally inhomogeneous sample images revealed a greater (2–5 times) sensitivity of the Stokes-correlometry method compared to the single-point approach.

The results of the study show than the direct Stokes polarimetry mapping can be a basis for the differential diagnosis of changes in optical anisotropy of the human biological tissues of different morphological structure and physiological state.

Acknowledgments

Ethical statement

The study design was approved by the Institutional Ethical Committee of Chernivtsi National University.

ORCID iDs

Motahareh Peyvasteh ⓘ https://orcid.org/0000-0001-7543-8320
Alexey Popov ⓘ https://orcid.org/0000-0002-1417-6715
Igor Meglinski ⓘ https://orcid.org/0000-0002-7613-8191

References

[1] Novikova T, Meglinski I, Ramella-Roman J C and Tuchin V V 2016 Polarized light for biomedical applications *J. Biomed. Opt.* **21** 071001
[2] Khlebtsov N G *et al* 2016 Introduction to light scattering by biological objects: extinction and scattering of light in disperse systems *Handbook of Optical Biomedical Diagnostics* ed V V Tuchin (Bellingham, WA: SPIE Press) ch 1 pp1–160
[3] Tower T T and Tranquillo R T 2001 Alignment maps of tissues: I. microscopic elliptical polarimetry *Biophys. J.* **81** 2954–63
[4] Ushenko A G and Pishak V P 2004 Laser polarimetry of biological tissue: principles and applications *Handbook of Coherent-Domain Optical Methods: Biomedical Diagnostics, Environmental and Material Science* vol 1 ed V V Tuchin (New York: Springer) pp 93–138
[5] Tuchin V V, Wang L and Zimnyakov D A 2006 *Optical Polarization in Biomedical Applications* (Berlin: Springer)
[6] Ghosh N and Vitkin I A 2011 Tissue polarimetry: concepts, challenges, applications and outlook *J. Biomed. Opt.* **16** 110801
[7] Pierangelo A, Benali A., Antonelli M -R, Novikova T, Validire P, Gayet B and De Martino A 2011 Ex-vivo characterization of human colon cancer by Mueller polarimetric imaging *Opt. Express* **19** 1582–93
[8] Das N K, Dey R, Chakraborty S, Panigrahi P K, Meglinski I and Ghosh N 2018 Quantitative assessment of submicron scale anisotropy in tissue multifractality by scattering Mueller matrix in the framework of Born approximation *Opt. Commun.* **413** 172–8
[9] Das N K, Dey R, Chakraborty S, Panigrahi P K, Meglinski I and Ghosh N 2018 Submicron scale tissue multifractal anisotropy in polarized laser light scattering *Laser Phys. Lett.* **15** 035601
[10] Kunnen B, Macdonald C, Doronin A, Jacques S, Eccles M and Meglinski I 2015 Application of circularly polarized light for non-invasive diagnosis of cancerous tissues and turbid tissue-like scattering media *J. Biophoton.* **8** 317–23
[11] Jacques S L 2011 Polarized light imaging of biological tissues *Handbook of Biomedical Optics* ed D Boas, C Pitris and N Ramanujam (Boca Raton, FL: CRC Press) pp 649–69
[12] Angelsky O V *et al* 2010 Statistical, correlation and topological approaches in diagnostics of the structure and physiological state of birefringent biological tissues *Handbook of Photonics for Biomedical Science* ed V V Tuchin (Boca Raton, FL: CRC Press) pp 283–322
[13] Ushenko Y A *et al* 2013 Diagnostics of structure and physiological state of birefringent biological tissues: statistical, correlation and topological approaches *Handbook of Coherent-Domain Optical Methods* ed V V Tuchin (New York: Springer) pp 107–48
[14] Ushenko V A and Gavrylyak M S 2013 Azimuthally invariant Mueller-matrix mapping of biological tissue in differential diagnosis of mechanisms protein molecules networks anisotropy *Proc. SPIE* **8812** 88120Y
[15] Ushenko V O 2012 Two-dimensional Mueller matrix phase tomography of self-similarity birefringence structure of biological tissues *Proc. SPIE* **8487** 84870W

J. Phys. D: Appl. Phys. **53** (2020) 395401

M Peyvasteh *et al*

[16] Ushenko V A, Pavlyukovich N D and Trifonyuk L 2013 Spatial-frequency azimuthally stable cartography of biological polycrystalline networks *Int. J. Opt.* **2013** 683174

[17] Ushenko Y A *et al* 2012 Spatial-frequency Fourier polarimetry of the complex degree of mutual anisotropy of linear and circular birefringence in the diagnostics of oncological changes in morphological structure of biological tissues *Quantum. Electron.* **42** 727–32

[18] Ellis J and Dogariu A 2004 Complex degree of mutual polarization *Opt. Lett.* **29** 536–8

[19] Ushenko V A 2013 Complex degree of mutual coherence of biological liquids *Proc. SPIE* **8882** 88820V

[20] Ushenko V A and Gorsky M P 2013 Complex degree of mutual anisotropy of linear birefringence and optical activity of biological tissues in diagnostics of prostate cancer *Opt. Spectrosc.* **115** 290–7

[21] Broky J and Dogariu A 2010 Complex degree of mutual polarization in randomly scattered fields *Opt. Express* **18** 20105–13

[22] Tervo J, Setala T and Friberg A 2009 Two-point stokes parameters: interpretation and properties *Opt. Lett.* **34** 3074–6

[23] Ushenko V O 2013 Spatial-frequency polarization phasometry of biological polycrystalline networks *Opt. Mem. Neural Netw.* **22** 56–64

[24] Ushenko Y A 2011 Investigation of formation and interrelations of polarization singular structure and Mueller-matrix images of biological tissues and diagnostics of their cancer changes *J. Biomed. Opt.* **16** 066006